Model Test Research on Pressure Wave in the Subway Tunnel

Haiquan Bi (bhquan@outlook.com)
Southwest Jiaotong University https://orcid.org/0000-0002-1892-2893
Yi Fang
Southwest Jiaotong University
Yuanlong Zhou
Southwest Jiaotong University
Honglin Wang
Southwest jiaotong University
Xu Zhang
Southwest Jiaotong University

Original Article

Keywords: Subway tunnel, Pressure wave, Model test, Intermediate air shaft, Bypass tunnel

Posted Date: December 29th, 2020

DOI: https://doi.org/10.21203/rs.3.rs-134821/v1

Model test research on pressure wave in the subway tunnel

Haiquan Bi *, Yi Fang, Yuanlong Zhou, Honglin Wang, Xu, Zhang

School of Mechanical Engineering, Southwest Jiaotong University, Chengdu 610031, China

* Corresponding Author: bhquan@outlook.com

Abstract

The pressure wave is of crucial importance for subway development since it greatly influences the comfort while taking. As the subway lines are rapidly developing in the cities, the pressure wave in different subway tunnel constructures is urgently needed to be studied and receded. In this paper, a subway tunnel pressure wave experimental system was designed, constructed, and tested. The influence of train model head shape, train model speed, shaft number in the tunnel, and bypass number in the tunnel on the pressure wave amplitude were experimented with and analyzed. The results show that the train model head shapes significantly impact the amplitude of the initial compression wave in the tunnel. The blunter train model head generates a greater amplitude of the initial compression wave. When the train passes through a single-track tunnel, the maximum positive pressure amplitude of the pressure wave in the tunnel is at the first compression wave at the tunnel entrance. The maximum negative pressure value in the tunnel is at the superposition of the initial compression wave reflected from the first time and the train's body, which is related to the length of the train's body, tunnel length, train's speed, and sound speed. The shaft set in the tunnel decreases the amplitude of the initial compression wave in the tunnel space behind, but it will increase the pressure wave's amplitude reflected in the tunnel when the train passes through the shaft. After the bypass tunnel is added, the initial compression wave propagation in the tunnel behind the bypass tunnel is receded. Still, it also increases the negative pressure amplitude when the train passes.

Key words: Subway tunnel; Pressure wave; Model test; Intermediate air shaft; Bypass tunnel

Nomenclature

φ	Diameter of traction rope and guide rope (mm)	S	The distance between the first and the second photoelectric switch (m)
M	Mach number	t	Time recorded by timer (s)
Re	Reynolds number	v_1	Velocity of train model to enter the tunnel (m/s)
ρ	Density of the air when the actual train is running	ρ'	Density of the air when the train model is running
V	Actual train velocity (km/h)	V'	Train model velocity (km/h)
L	Size of the actual train	L'	Size of the train model
μ	Dynamic viscosity coefficient of the air when the actual train is running	μ'	Dynamic viscosity coefficient of the air when the train model is running
S_1	Area of section 1 (m^2)	S_2	Windward area of train model (m^2)
$P_{P,1}$	Positive pressure peak of section 1 (Pa)	$P_{P,5}$	Negative pressure peak of section 1 (Pa)
$P_{N,5}$	Positive pressure peak of section 1 (Pa)	$P_{N,5}$	Negative pressure peak of section 5 (Pa)

1. Introduction

With the rapid development of the modern city scale, the number of urban populations is increasing, and the ground traffic is becoming more and more congested. To alleviate the urban traffic pressure, cities across the country are actively planning and building a more scientific and perfect traffic network system, among which, subway, one of the effective tools to relieve urban traffic pressure, has developed rapidly in recent years. By the end of 2019, 40 cities in China have opened 208 operating lines, with a total length of 6,736.2 kilometers. Besides, there are 279 subway lines under construction nationwide, with a total length of 6,902.5 kilometers.

When the train enters the tunnel, the internal air will be strongly squeezed by the train due to the closed space of the subway tunnel, and the gas at the tunnel entrance will be compressed, which leads to rapidly rising pressure, forming a pressure pulse [1][2]. As is shown in Fig 1, the phenomenon when the pressure pulse travels along the tunnel at speed close to that of sound is called compression wave [3]. When the compression wave reaches the entrance of the tunnel, part of it propagates to the outside of the tunnel, forming a so-called micro-pressure wave [4-5]; the other part is reflected back and propagates in the opposite direction [6], called expansion wave, which reflects again when it encounters the front of the car. This process is repeated, and a tunnel pressure wave is formed in the

tunnel [7]. The generation of pressure waves will greatly affect passengers' safety and comfort, as well as the normal operation of auxiliary equipment in the station [8].

The pressure wave generated by train operation is affected by many factors [14-17]. Among them, the shape of the front of the subway train greatly influences the amplitude of the pressure wave in the tunnel [18-19]. The train's running resistance with a blunt head is the largest, and the longer the shape of the head is, the smaller the resistance will be, but the slowing effect is gradually decreasing [20-21]. The peak value and gradient of the initial compression wave generated by the common CRH3 and CRH380A trains in China are also different at the same speed, the change of which in the CRH3 train is more severe than that of the CRH380A train [22]. Also, the velocity of the train has a great influence on the pressure wave. At present, most of the subway lines in China operate at 80 km/h. In recent years, 100 km/h and more than 100 km/h subway lines have been gradually put into operation, and many high-speed subways are under construction. After the subway speed reaches above 100km/h, many aerodynamic problems, especially the tunnel pressure wave [12-13]at the low speed of the subway, will be aggravated [9][10][11].

To prevent two trains from running in the tunnel at the same time, it is necessary to set up an intermediate air shaft in the interval tunnel when it is long [23]. Its function is to ensure that only one train runs in a ventilation section, avoiding multiple trains running when the breakdown of a certain vehicle or a fire may affect other vehicles [24]. Changing the basal area and position of the shaft set in the tunnel can effectively reduce the maximum pressure wave amplitude and gradient. The pressure wave amplitude will decrease as the basal area of the tunnel increases [25]. The optimal shaft position in the tunnel can make itself have the best decompression effect [26]. In addition, the height of the shaft also has a certain effect on the reduction of the pressure wave amplitude in the tunnel, which will decrease as the height of the shaft decreases [27].

The increase in the number of tunnels also has a great influence on the pressure wave in the subway tunnel [28]. For safety reasons, two tunnels connected with pressure relief pipes near the tunnel should be the first choice. When the train runs in a tunnel, the bypass tunnel can play a certain role of ventilation [29] and serve as a rescue channel in an emergency [30]. Therefore, it is necessary to study the effect of increasing bypass tunnels on pressure waves in the tunnel.

In this paper, the model test analyzes the influence of locomotive shape and running speed on the pressure wave. The influence of the number of shafts in the tunnel and the bypass tunnel is also studied. The second section of this paper introduces the working principle of the test system in detail.

The third section analyzes the errors in the model test. The fourth section analyzes the influence of various factors on the tunnel pressure wave. The last section draws the conclusion of this paper.

2. Model test

2.1 The bench of model test

2.1.1 Overview of the model test stand

Fig. 2(a) shows the main view of the schematic diagram of the pressure wave model test bench of this subway tunnel. The length of the tunnel model is 30.4m. The train model is 10 m from the tunnel entrance, and the deceleration section at the tunnel exit is 20 m long.

The three-dimensional view of the model test bench is shown in Figure 2(b). The model test bench mainly includes the drive wheel, tunnel model, driven wheel, two 3 mm guide ropes, one 3 mm traction rope which tows train model, brackets, and train model. The drive wheel is directly fixed on the output shaft of the variable frequency motor. The tunnel model is replaced with PVC pipes, and the mechanical fixing device of the tunnel is designed with the matching fixed clamp to fasten the pipe. Two φ 3 smooth wire ropes are fixed on the brackets at both ends at the same height and pass through the train model's body, which is used as the positioning track to determine the driving route of the train model. Traction rope uses φ 3 wire rope passing through drive wheel, driven wheel and tensioner wheel. The height of the tensioner wheel can be adjusted to achieve the tension of the traction rope. The train is connected to the traction rope, and the motor drives the drive wheel to rotate so as to drive the traction rope and train model.

The longitudinal section 1 of the tunnel when train model enters the tunnel is shown in Figure 3. The diameter of the tunnel's circular part is 0.31 m, the cross-sectional area of which is 0.0704714 m^2, and the width of the bottom is 0.2 m. The length of the model car is 1.4 m, the cross-sectional area of which is 0.01896 m^2. The train/tunnel area ratio is 0.269. The measuring points are arranged on the inner side of the pipeline with a horizontal distance of 0.14 m from the bottom.

2.1.2 Train operation system and its working principle

As is shown in Figure 4, the train operation system includes the launcher for train model, train model, motor, drive wheel, driven wheel, traction rope, guide rope, tensioner wheel and other equipment.

The working principle of the model test stand is as follows. Firstly, set the test speed in the PLC control system before the test, then press the launcher to separate the traction rope from the train model. Thirdly, control the motor to start working to drive the traction rope to accelerate it to the required traction speed. At this point, the release launcher connects the traction rope with the train model, driving the train model to run into the tunnel at speed required by the test in a short time. The two sensors at the entrance of the tunnel, which is shown in Fig. 5, detect the speed at which the model car enters the tunnel, and the sensor at the exit of the tunnel, which is shown in Fig. 6, monitors the speed at which the model car leaves the tunnel. Meanwhile, the pressure sensor arranged on the inner wall of the tunnel monitors the pressure generated by the train model. When the train model passes through the sensor at the exit, it will give a feedback signal to the PLC control system to stop the operation of the motor, which makes the traction wire rope to decelerate immediately, thus driving the train model to slow down at once after driving out and finally hit the buffer mechanism not far from the tunnel exit to stop completely for the next test.

The specific deceleration plan is as follows. As is shown in Fig. 6, the train's deceleration is realized by the motor brake and the train's connection multi-stage buffer device. When the train leaves the tunnel at high speed, the photoelectric switch, installed at the tunnel exit, senses and feeds back to the PLC. In the early stage, active deceleration is achieved through motor reversal and energy consumption braking given by frequency converter controlled by PLC, while in the later stage, the train is decelerated passively by setting a multi-stage buffer sponge. Two kinds of deceleration not only protect the body but also achieves an efficient speed reduction. When the test is completed, the motor is reversed at low speed to allow the train to run from the tunnel exit to the tunnel entrance to achieve rapid train recovery.

2.2 Test instrument

2.2.1 Pressure Sensor

As is shown in Fig. 7, this test uses a durable, robust miniature piezoresistive pressure sensor with high sensitivity- Endevco® model 8515C-15. Its surface mounting thickness is only 0.76mm, and the diameter is 6.3mm. The Endevco® model 8515C-15 can be installed on curved surfaces due to its small dimensions, with little disturbance to laminar or hot airflow, and installed in grooves on the test surface. Therefore, the pressure sensor is widely used in local pressure measurement in wind tunnel tests and surface aerodynamic measurement in flight test.

2.2.2 Data collection system

As is shown in Fig. 8, this test uses DTS's SLICE to collect test data. SLICE is an ultra-small modular data acquisition system with excellent flexibility, technology, and reliability. The basic module BASE SLICE of the data acquisition system contains a microprocessor, memory, and control circuit. It can be connected to a computer and a pressure sensor at the same time. Besides, the acquisition system uses supporting SLICEWare software to complete sensor information storage and data acquisition. During the test, the pressure sensor sensing the pressure signal converts it into an electrical signal, and the pressure value is displayed in the computer test supporting software after being processed in the data acquisition system.

2.2.3 Train speed test system

The train speed test scheme is shown in Fig. 5. Two diffused photoelectric switches of the same type and batch are arranged in front of the tunnel entrance at a distance of S and are connected to two high-speed counter ports of PLC. When the train passes the first photoelectric switch at high speed, the counting of the first high-speed counter is interrupted, and the PLC immediately enters the interrupt program to start the timer. At this time, the train's speed entering the tunnel is the ratio of S to the time t just recorded by the timer, i.e., v1 = S/t. Fig. 9 shows the appearance of the photoelectric switch.

During the test, a Programmable logic controller (hereinafter referred to as PLC) controls the motor operation, speed setting, and train recovery. Fig. 10 shows the operation interface of PLC in which the acceleration time, deceleration time, and the reverse time for the motor to decelerate are set. Taking the first photoelectric switch position in Figure 5 as the reference, position 1 for velocity measurement is where the velocity sensor at the entrance lies, and position 2 is where the velocity sensor at the exit lies. The train model's speed entering the tunnel is determined by the distance value entered at position 1 for velocity measurement in the PLC and the time difference between the first photoelectric switch and the second photoelectric switch. Similarly, the speed of the train model exiting the tunnel can be obtained. The two speeds can be shown on the interface in Figure 10. Before we start a new test, the speed required for the test is set on the equipment. When we click the start button, the motor starts to run, driving the traction system, and the real-time speed is displayed on the interface. When the model car passes through the sensor at the tunnel's exit, the PLC receives the

signal and immediately controls the motor to stop and decelerate by reversing. During the test, you can also press the stop button to stop the motor immediately.

2.3 Layout of measuring points

Fig. 11 is a schematic diagram of the arrangement of each pressure measuring point in this test. In this test, a total of 6 test sections were arranged along the tunnel, and the distance between each was 3.8m. Specifically, Fig. 11(a) shows the arrangement of measuring points under the condition of no shaft and no bypass tunnel. Fig. 11(b) and Fig. 11(c) show the schematic diagram of the measuring point layout when one and two shafts are set without a bypass tunnel. Fig. 11(d) and Fig. 11(e) show the schematic diagrams of measuring point layout when testing one and two bypass tunnels without shafts.

2.4 Determination of similarity criterion

Certain similar conditions must be met to make the test data comparable and useful in the scale model experiment, which includes the similarity of dynamics, geometry, and motion [31]. The thermal similarity when the train enters the tunnel is temporarily ignored because the energy loss and temperature change are minimal.

It is vital to consider the dynamic similarity criterion because geometric motion similarity is easily satisfied. When simulating gas flow in a tunnel, the two most important parameters are the Mach number (hereinafter referred to as M) and the Reynolds number (hereinafter referred to as Re).The physical meaning of Re is the ratio of characteristic inertial force to viscous force, namely

$$\mathrm{Re} = \frac{\rho V^2/L}{\mu V/L^2} = \frac{\rho VL}{\mu} \tag{1}$$

Re is a similar criterion that reflects the effect of fluid viscosity on flow. If the two flow fields are similar, the effect of inertia force and viscous force should be the same, so is the Reynolds number of the two flow fields the Reynolds number of the two flow fields.

$$\mathrm{Re} = \frac{\rho VL}{\mu} = \mathrm{Re}' = \frac{\rho' V' L'}{\mu'} \tag{2}$$

In this formula, ρ is the density of the air when the actual train is running, V is the velocity of the actual train, L is the size of the actual train, and μ is the dynamic viscosity coefficient of the air. ρ' is the density of the air when the train model is running, V' is the speed of train model, L' is the size of

196 the actual train, and μ' is the dynamic viscosity coefficient of the air. In the model test, ρ/μ is related
197 to the ambient temperature of the test site. So, when the temperature has less changes, ρ/μ can be
198 regarded as a fixed value. Therefore, V and L should be equal to make Re equal. If the Re is to be
199 equal, the speed of the train model should be higher than 20 times the actual train speed because the
200 size similarity ratio of the model is less than 1/20, which cannot be achieved in the model test.

201 However, people found that in applying the dynamic similarity criterion, the flow field has a
202 "self-modeling region" [32]. The phenomenon that the flow state and velocity distribution are similar
203 to each other and not depend on the Re's change when it is in a certain range is called "self-modeling".
204 When Re is less than a certain value (the first critical value), the flow is laminar. When it is greater
205 than the first critical value, the flow changes from laminar to turbulent flow. It gradually enters a
206 turbulent state when the change of Re has a greater impact on the flow state and velocity distribution.
207 When Re increases to a certain value (the second critical value), the flow state and velocity
208 distribution are similar to each other and do not change with the change of the Re. That is, the flow
209 enters the " self-modeling region ", and the corresponding flow is fully developed turbulence. When
210 the train model and the actual train are in the same self-modeling region, the model test results can be
211 used in the actual object. Because the speed range studied here belongs to subsonic speed and is
212 already in a highly turbulent state, it can be considered that the flow field is in the self-model region.
213 At this time, researchers can start the model test without considering the restriction of Re's similarity
214 condition.
215

216 ## 3. Error analysis

217 In the test process, various links will produce certain errors, which will lead to deviations in the
218 experimental results. The major influencing factors are the sensor's errors, the running speed of the
219 train model, and the test environment temperature.

220 Before the start of this model test, pressure sensors used in the test have been calibrated in the
221 national legal metrological verification agency. The calibration method is as follows. During the
222 calibration process, the pressure sensor was placed in the calibration environment for more than 2
223 hours. Then the pressure sensor and the standard digital pressure gauge were installed on the pressure
224 pump at the same time. Starting from the lower measurement limit of the pressure sensor, according to
225 the calibration point setting, the pressure was raised to the upper limit of measurement point by
226 point. Then the pressure was reduced from the upper measurement limit point by point to the lower

measurement limit. During this process, the output value of the pressure sensor was recorded in turn. Finally, the basic error of the pressure sensor was within ± 0.2%. A standard voltage value which is input into the data acquisition system is compared with the actual voltage value reading, the error of the which is within 0.5%.

In this test, the PLC control system controls the motor to reach the required rotation speed, and the traction rope is pulled to accelerate to the required speed. And the train model and the traction rope are combined to run at the test speed. Before the start of the test, different operating speeds are set in the PLC control system, and the passing time of the train model is tested and recorded by sensors installed at the entrance and exit of the tunnel. Therefore, the actual running speed of the model car is calculated. Speed errors are all within 1% through multiple comparisons between the set running speed and the actual measured speed.

The model test bench is set up in an indoor laboratory to minimize the impact of the test environment on this test. As shown in Table 1, the on-site ambient temperature is recorded before each test, and the maximum change in each case doesn't exceed 10%. For the same test case, the experimental data are obtained after repeated testing three times, the relative error of whose pressure amplitude is within 3%.

4. Results and Discussion

The pressure wave in the tunnel is affected by many factors. This paper mainly discusses the influence of the shape of the train's head, train speed, the establishment of the shaft, and the bypass tunnel in the tunnel on the pressure wave.

4.1 The influence of the shape of locomotive on the tunnel pressure wave

Differentiation in the locomotive's shape will affect the amplitude and maximum positive and negative pressure wave extremum formed when the train enters the tunnel. In order to study the influence of trains with different locomotive shapes on the pressure wave in the tunnel, train models with locomotive angles of 45°, 60°, and 75° were used in the test. Fig. 12 shows the schematic diagram of the train model in each test case. The train model's length is 1.4m, and the cross-sectional area is the same.

Detailed parameters of each train are given in Table 2. During the test, the model train's running speed is 80 km/h, and the model tunnel is not equipped with intermediate air shafts and bypass

tunnels.

Figure 13 shows the dynamic pressure change curve of measuring point 1. The first wave crest and wave trough are generated when the model train's head and tail pass the tunnel entrance, respectively. It can be seen that with the increase of locomotive angle, the amplitude of the initial pressure wave generated by the train model passing through the tunnel also increases gradually, among which the pressure amplitude of the train model with 75 ° locomotive head is the largest, reaching 400 Pa.

Fig. 14 shows the comparison of the aerodynamic pressure peaks at different measuring points of the three different car head shapes when passing through the model tunnel. Fig. 14(a) shows the positive pressure peak, Fig. 14(b) shows the negative one. It can be seen from the figure that with the increase of the train head angle, the maximum positive and negative values generated by the train passing through the measuring points are increased. It can be seen from Table 2 that the windward area of the front of the car decreases with the increase of the angle of the windward surface, thus increasing the resistance encountered by the air flowing through the front and increasing the positive amplitude of the initial compression wave.

4.2 The influence of train speed on tunnel pressure wave

The size of the initial compression waves generated when the subway enters the tunnel depends on the train's speed. This section studies the variation of aerodynamic pressure generated when the model train passes through the model tunnel at different speeds to study the influence of velocity on compression waves. During the test, a train model with a head angle of 60° was used, and the tunnel model was not equipped with an intermediate air shaft and a bypass tunnel.

Figure 15 shows each section wall's pressure amplitude when the train model passes through the tunnel at three different speeds (60 km/h, 70 km/h, 80 km/h). The measuring point with the largest positive pressure amplitude is point 1, arranged on section 5.7m away from the tunnel entrance. The maximum positive pressures at three speeds (60 km/h, 70 km/h, 80 km/h) are 172 pa, 228 pa, and 280 pa, respectively. The measuring point with the largest negative pressure amplitude is on the section 9.5 m away from the tunnel entrance. The maximum negative pressure amplitudes at the three speeds are -142 Pa, -240 Pa, and -305 Pa.

The positive pressure fluctuation in the tunnel is generated by the compressed air when the train model enters the tunnel and will gradually decrease along the tunnel model's length due to the

influence of the tunnel model wall friction and running resistance. Therefore, the maximum positive pressure value monitored by the measuring point in the tunnel model is located in section 1. The compression wave formed by the train model entering the tunnel model will propagate in the tunnel model at speed close to that of sound and propagate back when an expansion wave is generated at the exit, propagating back and forth in the tunnel. An expansion wave will be generated when the rear of the car enters the tunnel, whose propagation path is the same as the compression wave. A large negative pressure is generated when the train model passes through the measuring point because the pressure will be superimposed when the expansion wave propagating back and forth in the tunnel encounters the car body. Figure 16 shows the analysis diagram of pressure fluctuations in the tunnel model. It can be seen from Figure 16 that when the train model passes through Section 2 or Section 3, it encounters the expansion wave propagating in the tunnel model, making the negative pressure value at this point larger. Therefore, the theoretical analysis is consistent with the experimental results.

It can also be seen from Figure 15 that the positive and negative pressure amplitudes of each measuring point increase as the speed of the train model increases. Select the data at the measurement points of Section 1 and Section 5 for function fitting. It can be seen from Figure 17 that the pressure value at the measuring point is proportional to the square of the train model speed.

4.3 Influence of shaft on pressure wave in tunnel

The tunnel structure changes after the intermediate air shafts are installed in the interval tunnel, so it is necessary to analyze the influence of the intermediate air shaft on the change of the tunnel pressure wave. This section examines this effect. The conditions of one and two wind shafts are set up in the model tunnel, respectively, for research, whose positions are shown in Figure 11(b) and Figure 11(c). During the test, the diameter of the shaft is 0.11 m, and the height is 2.6 m, and a model train with a head shape of 60° was used, running speed of which was 80km/h, and no bypass tunnel was set in the model tunnel.

Figure 18 shows the dynamic pressure curve of the initial compression wave at section 1 when the train enters the tunnel under three different working conditions, namely, the shaft number is 0, 1, and 2. Under the three working conditions, the positive pressure amplitude of the initial compression wave is 287 Pa, 281 Pa, and 278 Pa, respectively, with a small difference in the peak value of the pressure wave due to the air wells set after section 1. Therefore, whether a shaft is set in the tunnel has little influence on the initial pressure wave at the tunnel entrance.

Fig. 19 shows the dynamic change curve of the pressure wave on point 3. Under the three working conditions, the positive pressure amplitude of the initial compression wave is 300Pa, 244 Pa, and 233 Pa, respectively, with little change, and the negative one is -177Pa, -128 Pa, and -137 Pa. However, when the train model passes through the first shaft, it can be seen that the pressure amplitude of the measuring point is the largest under the condition of setting a shaft while the smallest under no shaft. This is because the measuring point is behind the first vertical shaft. When the train model passes through the shaft, not only the compression wave is not reduced, but the pressure fluctuation is increased.

Fig. 20 shows the dynamic change curve of the pressure wave on section 4. Under the three working conditions, the positive pressure amplitude of the initial compression wave is 285 Pa, 230 Pa, and 198 Pa, respectively, with little change, and the negative one is -170 Pa, -146 Pa, and -177 Pa. When the train model passes through the first shaft, the rule is the same as that in the measuring point of section 3. When the model train passes through the second shaft, it can be seen that the pressure amplitude of the measuring points in the working conditions under two shafts has also increased, which is similar to the situation when a model train passes through the first shaft. The reason for this phenomenon is the increase of the air shaft's number. When the train passes through the shaft, a pressure wave will be generated and superimposed with the pressure wave reflected in the tunnel so that the pressure monitored at the measuring point will increase.

It can be clearly seen from Fig. 18, Fig. 19, and Fig. 20 that when the train model passes through the measuring point, the amplitude of negative pressure generated under the condition of one shaft and two shafts is larger than that under the condition of no shaft. The reason for this phenomenon is that the air velocity in the tunnel increases with the increase of the shaft, and the negative pressure generated by the train passing through the measuring point also increases due to the existence of the shaft. The pressure wave will also be superimposed with the negative pressure of the train passing by, making the pressure amplitude increase or decrease, which is related to the shaft position, train speed, and tunnel length.

4.4 Influence of Bypass Tunnel on Tunnel Pressure Wave

This section studies the influence of the number of bypass tunnels on the pressure wave in the tunnel. The conditions are studied by setting 1 and 2 bypass tunnels in the tunnel model. The layouts of measuring points are shown in Figure 11(d) and figure 11(e). During the test, the diameter of the

bypass tunnel is 0.25 m, and a model train with a head shape of 60° was used, the running speed of which was 80 km/h. No air shaft was set in the tunnel model.

Figure 21 shows the pressure dynamic change curve at the measuring point of section 1 when the train model passes through the tunnel model under three different conditions, that is, straight, one bypass, and two bypass tunnels. The positive pressure amplitudes of the initial compression wave under the three test conditions are 286 Pa, 264 Pa, and 250 Pa, and the negative ones are -100 Pa, -40 Pa, and -30 Pa, respectively. The positive pressure of the initial compression wave changes little, but the negative pressure amplitude decreases with the increase of the bypass tunnel at measuring point 1, which indicates that the increased bypass tunnel plays a role in reducing the negative pressure amplitude of the initial compression wave. The reason for this phenomenon is that the initial compression wave generated by the front of the train model is reflected back and forth in the tunnel between the bypass tunnel and the tunnel entrance, and the expansion wave generated at the measuring point 1 and the rear of the vehicle entering the tunnel is just superimposed to offset, which makes the negative pressure amplitude of the initial compression wave decrease.

Figure 22 shows the pressure dynamic change curve of the measuring point in test section 5. The positive pressure amplitudes of the initial compression wave under the three working conditions are 275 Pa, 245 Pa, and 186 Pa and the negative ones are -165 Pa, -130 Pa, and -22 Pa, which means both the positive pressure amplitude and negative pressure amplitude of the initial compression wave have decreased. This is because after the bypass tunnel is added when the initial compression wave passes through the bypass tunnel, the air flowable area in the tunnel increases, which has a certain pressure relief effect on the initial compression wave. However, when the train model passed the measuring point, the negative pressure amplitudes were -189 Pa, -250 Pa, and -230 Pa, respectively, which shown the increase of the bypass tunnel increased the pressure amplitude change in the tunnel.

Figure 23 shows the dynamic pressure change curve at the measuring points of the test section 6. It can be seen that the change rule of the initial compression wave is consistent with that of section 5. The increase of the bypass tunnel slows down the amplitude of the initial compression wave, and the mitigation effect of two bypass tunnels is greater than that of one bypass tunnel. When the train model passes through the measuring points of three different structure tunnels (no bypass tunnel, one bypass tunnel, and two bypass tunnels), the negative pressure amplitudes generated are -227 Pa, -300 Pa, and -306 Pa, respectively. The results are the same as those on section 5 similar. The main reason is that the air circulation area becomes larger after the bypass tunnel is added, and the drag coefficient

encountered by the model car when traveling decreases, which will increase the air velocity and static pressure at the section.

5. Conclusion

This paper uses the research method of model test to study the influence factors of the pressure wave in the subway tunnel by analyzing the influence of the locomotive shape, the speed of the train, the middle air shaft, and the bypass tunnel on the change rule of the pressure wave in the tunnel. The main conclusions are as follows:

(1) When the train runs at a speed of 80 km/h, the blunter the locomotive shape is, the larger the initial compression is. The pressure amplitude generated by the locomotive angle of 75° is 43.6 % higher than that generated by the 60° locomotive angle.

(2) After the train enters the tunnel from outside, the place with the largest positive pressure amplitude of the pressure wave is the tunnel entrance, and the amplitude will continuously attenuate along the tunnel length. The maximum negative pressure amplitude is related to the length of the tunnel and the train as well as the train itself. When the train encounters the expansion, a wave reflected back and forth in the tunnel as the train is running, the negative pressure amplitude will increase and may become the maximum one.

(3) After the middle air shaft is set in the tunnel, the amplitude of the initial compression wave in the tunnel space in front of the air shaft is less slow down, and the amplitude of the initial compression wave in the space behind the air shaft will be slowed down, but the amplitude value of the pressure wave propagating in the space behind the air shaft will be enhanced.

(4) After the bypass tunnel is added to the tunnel, the positive pressure amplitude of the initial compression wave will not be affected for the tunnel space in front of the bypass tunnel, but the negative pressure amplitude will be affected due to the reflection of the initial compression wave propagating to the bypass tunnel, and the specific impact is related to the train length, tunnel length and train speed. For the tunnel space behind the bypass tunnel, the set of bypass the tunnel will slow down the impact of the initial compression wave but will enhance the amplitude of negative pressure generated by the train passing by.

Declarations

Data Availability Statement

The raw/processed data required to reproduce these findings cannot be shared at this time as the data also forms part of an ongoing study.

Competing interests

We declare that we have no financial and personal relationships with other people or organizations that can inappropriately influence our work, there is no professional or other personal interest of any nature or kind in any product, service and/or company that could be construed as influencing the position presented in, or the review of, the manuscript entitled, “Model Test Research on Pressure Wave in Metro Tunnel”.

Funding

The authors are grateful to the National Natural Science Foundation of China for its financial contribution to the project [grant number 51808460] and to the Fundamental Research Funds for the Central Universities [grant number 2682019CX32].

Authors' contributions

Haiquan Bi, Yi Fang contributed to the conception of the study;

Yi Fang, Xu Zhang performed the experiment;

Haiquan Bi, Yuanlong Zhou contributed significantly to analysis and manuscript preparation;

Honglin Wang, Yuanlong Zhou performed the data analyses and wrote the manuscript;

Haiquan Bi, Yi Fang helped perform the analysis with constructive discussions.

Acknowledgements

Not applicable.

References

[1] Zhang, L., Yang, M., Liang, X., Zhang, J., 2017. Oblique tunnel portal effects on train and tunnel aerodynamics based on moving model tests. Journal of Wind Engineering and Industrial Aerodynamics 167, 128–139. https://doi.org/10.1016/j.jweia.2017.04.018

[2] Li, Z., Yang, M., Huang, S., Liang, X., 2017. A new method to measure the aerodynamic drag of high-speed trains passing through tunnels. Journal of Wind Engineering and Industrial Aerodynamics 171, 110–120. https://doi.org/10.1016/j.jweia.2017.09.017

[3] Zhang, G., Kim, D.H., Kim, H.D., 2018. Numerical studies on the radiation of train-tunnel impulse waves. Tunnelling and Underground Space Technology 80, 211–221. https://doi.org/10.1016/j.tust.2018.06.020

[4] Zhang, L., Thurow, K., Stoll, N., Liu, H., 2018. Influence of the geometry of equal-transect oblique tunnel portal on compression wave and micro-pressure wave generated by high-speed trains entering tunnels. Journal of Wind Engineering and Industrial Aerodynamics 178, 1–17. https://doi.org/10.1016/j.jweia.2018.05.003

[5] Xiang, X., Xue, L., Wang, B., Zou, W., 2018. Mechanism and capability of ventilation openings for alleviating micro-pressure waves emitted from high-speed railway tunnels. Building and Environment 132, 245–254. https://doi.org/10.1016/j.buildenv.2018.01.045

[6] Soper, D., Gillmeier, S., Baker, C., Morgan, T., Vojnovic, L., 2019. Aerodynamic forces on railway acoustic barriers. Journal of Wind Engineering and Industrial Aerodynamics 191, 266–278. https://doi.org/10.1016/j.jweia.2019.06.009

[7] Iliadis, P., Soper, D., Baker, C., Hemida, H., 2019. Experimental investigation of the aerodynamics of a freight train passing through a tunnel using a moving model. Proceedings of the Institution of Mechanical Engineers, Part F: Journal of Rail and Rapid Transit 233, 857–868. https://doi.org/10.1177/0954409718811736

[8] Raghunathan, R.S., 2002. Aerodynamics of high-speed railway train. Progress in Aerospace Sciences 46. https://doi.org/10.1016/j.tust.2019.01.009

[9] Raghunathan, R.S., Kim, H.D., Setoguchi, T., 2002. Aerodynamics of high-speed railway train. Progress in Aerospace Sciences, 38, 469-514. https://doi.org/10.1016/S0376-0421(02)00029-5

[10] Ko, Y.-Y., Chen, C.-H., Hoe, I.-T., Wang, S.-T., 2012. Field measurements of aerodynamic pressures in tunnels induced by high speed trains. Journal of Wind Engineering and Industrial Aerodynamics 100, 19–29. https://doi.org/10.1016/j.jweia.2011.10.008

[11] Khayrullina, A., Blocken, B., Janssen, W., Straathof, J., 2015. CFD simulation of train aerodynamics: Train-induced wind conditions at an underground railroad passenger platform. Journal of Wind Engineering and Industrial Aerodynamics 139, 100–110. https://doi.org/10.1016/j.jweia.2015.01.019

[12] William-Louis, M., Tournier, C., 2005. A wave signature based method for the prediction of pressure transients in railway tunnels. Journal of Wind Engineering and Industrial Aerodynamics 93, 521-531. https://doi.org/10.1016/j.jweia.2005.05.007

[13] Zhang, L., Yang, M., Niu, J., Liang, X., Zhang, J., 2019. Moving model tests on transient pressure and

micro-pressure wave distribution induced by train passing through tunnel. Journal of Wind Engineering and Industrial Aerodynamics 191, 1–21. https://doi.org/10.1016/j.jweia.2019.05.006

[14] Yuan, H., Zhou, D., Meng, S., 2019. Study of the unsteady aerodynamic performance of an inter-city train passing through a station in a tunnel. Tunnelling and Underground Space Technology 86, 1–9. https://doi.org/10.1016/j.tust.2019.01.009

[15] Mei, Y., 2013. A Generalized Numerical Simulation Method for Pressure Waves Generated by High-Speed Trains Passing through Tunnels. Advances in Structural Engineering 16, 1427–1436. https://doi.org/10.1260/1369-4332.16.8.1427

[16] Zhou, D., Tian, H., Zhang, J., Yang, M., 2014. Pressure transients induced by a high-speed train passing through a station. Journal of Wind Engineering and Industrial Aerodynamics 135, 1–9. https://doi.org/10.1016/j.jweia.2014.09.006

[17] Liu, T., Jiang, Z., Li, W., Guo, Z., Chen, X., Chen, Z., Krajnovic, S., 2019. Differences in aerodynamic effects when trains with different marshalling forms and lengths enter a tunnel. Tunnelling and Underground Space Technology 84, 70–81. https://doi.org/10.1016/j.tust.2018.10.016

[18] Chen, X.-D., Liu, T.-H., Zhou, X.-S., Li, W., Xie, T.-Z., Chen, Z.-W., 2017. Analysis of the aerodynamic effects of different nose lengths on two trains intersecting in a tunnel at 350 km/h. Tunnelling and Underground Space Technology 66, 77–90. https://doi.org/10.1016/j.tust.2017.04.004

[19] Niu, J., Zhou, D., Liu, F., Yuan, Y., 2018. Effect of train length on fluctuating aerodynamic pressure wave in tunnels and method for determining the amplitude of pressure wave on trains. Tunnelling and Underground Space Technology 80, 277–289. https://doi.org/10.1016/j.tust.2018.07.031

[20] Wang, J.-Y.,2006. Aerodynamic study on the high-speed railway tunnel with large cross-sections. Thesis of master. Southwest Jiaotong University, Chengdu, China.

[21] Heine, D., Ehrenfried, K., Heine, G., Huntgeburth, S., 2018. Experimental and theoretical study of the pressure wave generation in railway tunnels with vented tunnel portals. Journal of Wind Engineering and Industrial Aerodynamics 176, 290–300. https://doi.org/10.1016/j.jweia.2018.03.020

[22] Wang, R.-L.,2015. Numerical study on aerodynamic effect of high speed train entering tunnel. Thesis of master.

Lanzhou Jiaotong University, Lanzhou, China.

[23] Ran, T., Xiong, X., 2017. Study of the Change of the Shaft Shape on the Influence to Aerodynamics Effect of the High-Speed Metro Tunnel. DEStech Transactions on Engineering and Technology Research. 2475-885X,678-687.
https://doi.org/10.12783/dtetr/icia2017/15691

[24] Fujii, K., Ogawa, T., 1995. Aerodynamics of high speed trains passing by each other. Computers & Fluids 24, 897–908.
https://doi.org/10.1016/0045-7930(95)00024-7

[25] Xiong, X., Zhu, L., Zhang, J., Li, A., Li, X., Tang, M., 2020. Field measurements of the interior and exterior aerodynamic pressure induced by a metro train passing through a tunnel. Sustainable Cities and Society 53, 101928.
https://doi.org/10.1016/j.scs.2019.101928

[26] Li Z.-W., Liang X.-F., Zhang J, 2011. Influence of shaft on alleviating transient pressure in tunnel. Journal of Central South University (Science and Technology)42, 2514–2519.

[27] Li Z.-W., Liang X.-F., Zhang J.,2 010. Study of alleviating transient pressure with cross passage in a tunnel. Journal of Railway Science and Engineering 7, 37–41.

[28] Li, X.-Z., Wang, M., Xiao, J., Zou, Q.-Y., Liu, D.-J., 2018. Experimental study on aerodynamic characteristics of high-speed train on a truss bridge: A moving model test. Journal of Wind Engineering and Industrial Aerodynamics 179, 26–38.
https://doi.org/10.1016/j.jweia.2018.05.012

[29] Baron, A., Mossi, M., Sibilla, S., 2001. The alleviation of the aerodynamic drag and wave effects of high-speed trains in very long tunnels. Journal of Wind Engineering and Industrial Aerodynamics 89, 365–401.
https://doi.org/10.1016/S0167-6105(00)00071-4

[30] Zhang, H., Zhu, C., Liu, M., Zheng, W., You, S., Li, B., Xue, P., 2017. Mathematical modeling and sensitive analysis of the train-induced unsteady airflow in subway tunnel. Journal of Wind Engineering and Industrial Aerodynamics 171, 67–78.
https://doi.org/10.1016/j.jweia.2017.09.005

[31] Heine, D., Ehrenfried, K., Kühnelt, H., Lachinger, S., Rudolph, M., Vorwagner, A., Saliger, F., 2019. Influence of the shape and size of cavities on pressure waves inside high-speed railway tunnels. Journal of Wind Engineering and Industrial Aerodynamics 189, 258–265.
https://doi.org/10.1016/j.jweia.2019.03.032

[32] Xu, Y.-H., Mu, S.,1990. Basic fluid experiment. Fudan University Press, Shanghai.

Fig. 1. Schematic diagram of pressure wave caused by train passing through tunnel.

Fig. 2. Schematic diagram of the model test bench. (a) Main view of the bench.

Fig. 2. Schematic diagram of the model test bench. (b) Three-dimensional view of the bench.

Fig. 3. The longitudinal section 1 of the tunnel when train model enters the tunnel.

Fig. 4. Main units' diagram of train operation system. (a) The launcher for train model.

Fig. 4. Main units' diagram of train operation system. (b) The train model.

Fig. 4. Main units' diagram of train operation system. (c) The drive wheel and the motor.

Fig. 4. Main units' diagram of train operation system. (d) The driven wheel.

Fig. 4. Main units' diagram of train operation system. (e) The tensioner wheel.

Fig. 5. Sensors at tunnel entrance.

Fig. 6. Damping system of the model test bench. (a) Sensor at tunnel exit.

Fig. 6. Damping system of the model test bench. (b) The buffer structure of tunnel exit.

Fig. 7. Pressure sensor Endevco® model 8515C-15.

Fig. 8. Data acquisition system SLICE.

Fig. 9. Photoelectric switch.

Fig. 10. The interface of PLC control system.

Fig. 11. Layout of measuring points in tunnels (the circles in the figure are the measuring points arranged). (a) No shaft, no bypass tunnel.

Fig. 11. Layout of measuring points in tunnels (the circles in the figure are the measuring points arranged). (b) 1shaft，no bypass tunnel.

Fig. 11. Layout of measuring points in tunnels (the circles in the figure are the measuring points arranged). (c) 2shaft，no bypass tunnel.

Fig. 11. Layout of measuring points in tunnels (the circles in the figure are the measuring points arranged). (d) 1 bypass tunnel，no shaft

Fig. 11. Layout of measuring points in tunnels (the circles in the figure are the measuring points arranged). (e) 2 bypass tunnel，no shaft

Fig. 12. Comparison of locomotive of different shapes.

Fig. 13. Comparison of dynamic pressure changes at measuring point 1.

Fig. 14. Pressure peaks generated by the train models with different head shapes. (a) Positive pressure values.

Figures

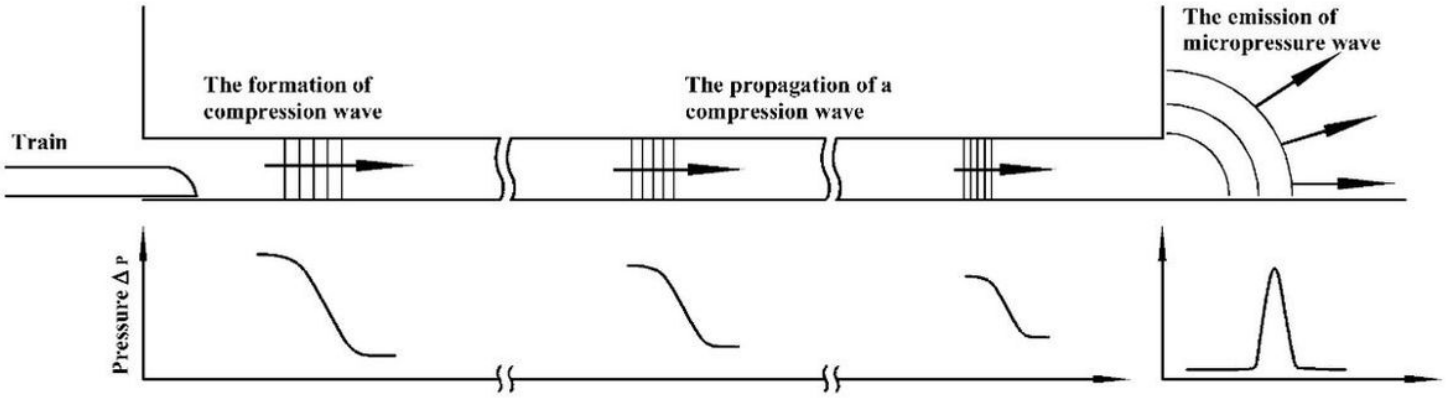

Figure 1

Schematic diagram of pressure wave caused by train passing through tunnel

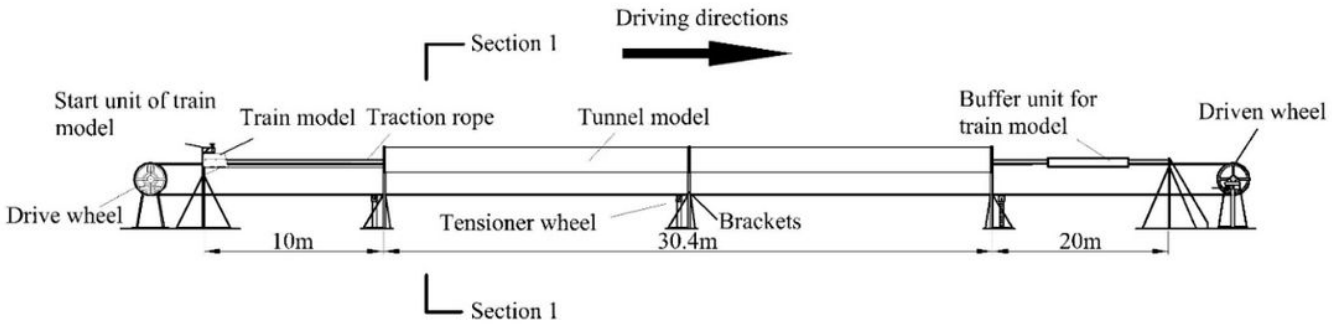

(a) Main view

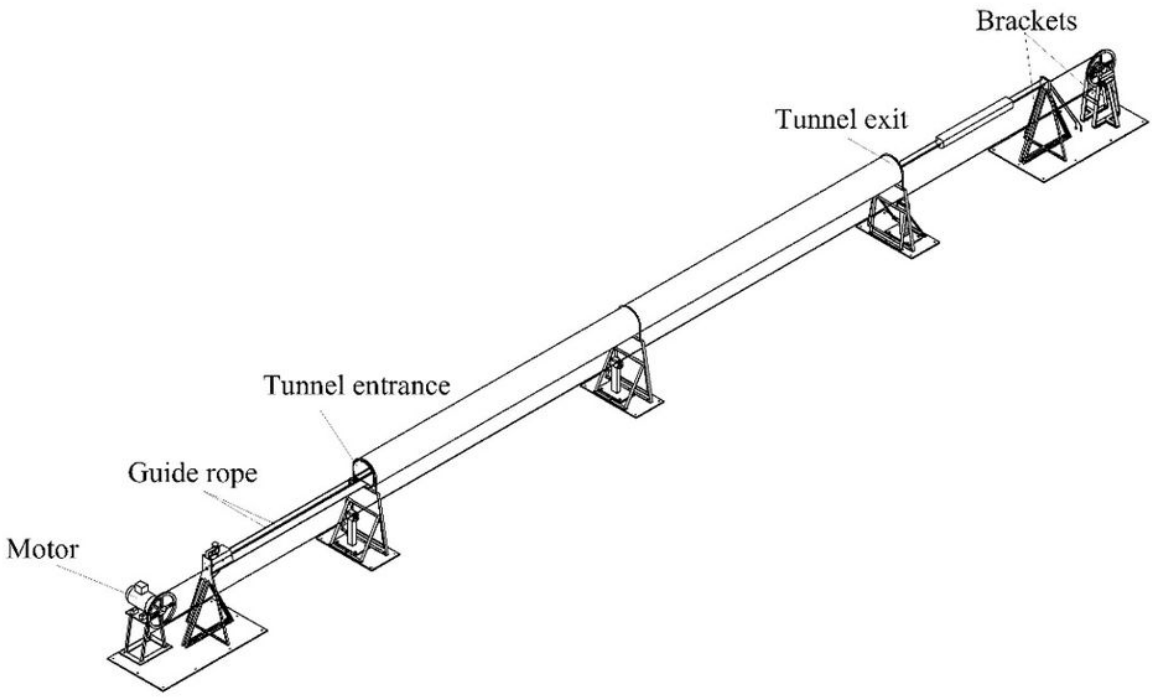

(b) Three-dimensional view

Figure 2

Schematic diagram of the model test bench

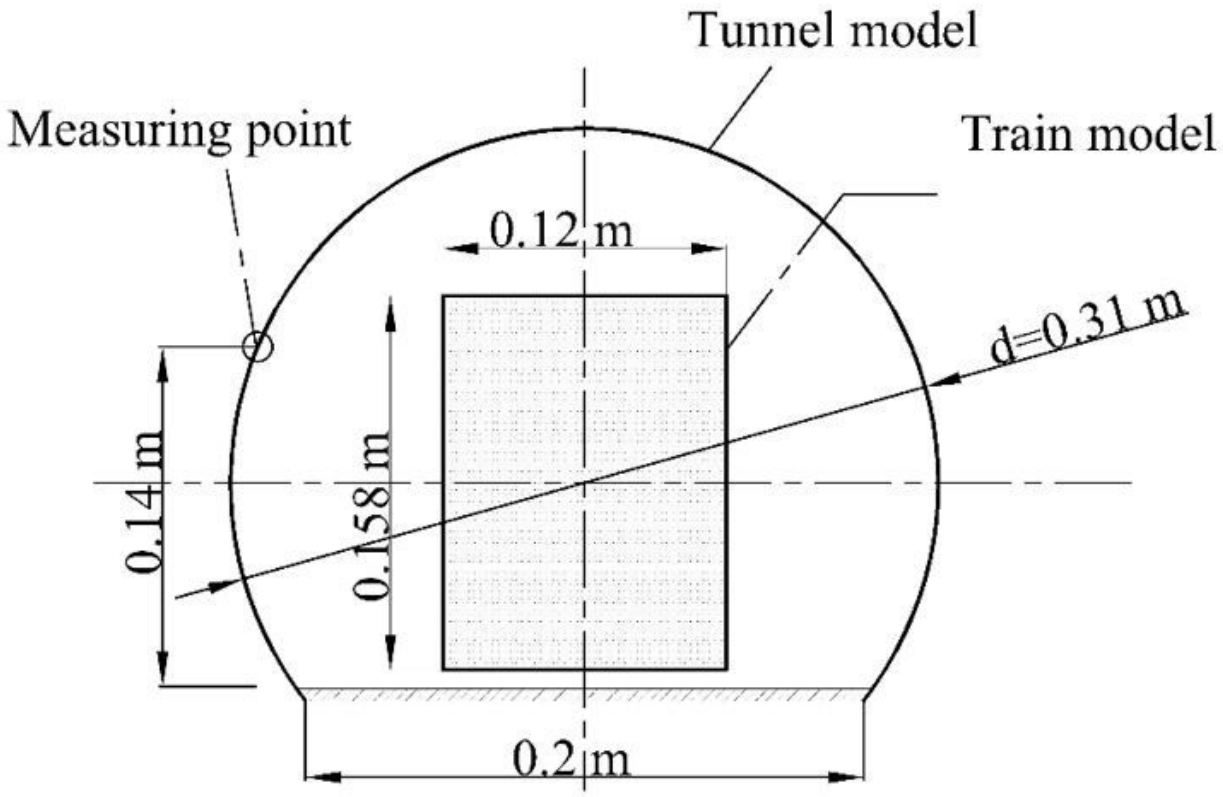

Figure 3

The longitudinal section 1 of the tunnel when train model enters the tunnel

Figure 4

Main unit of train operation system

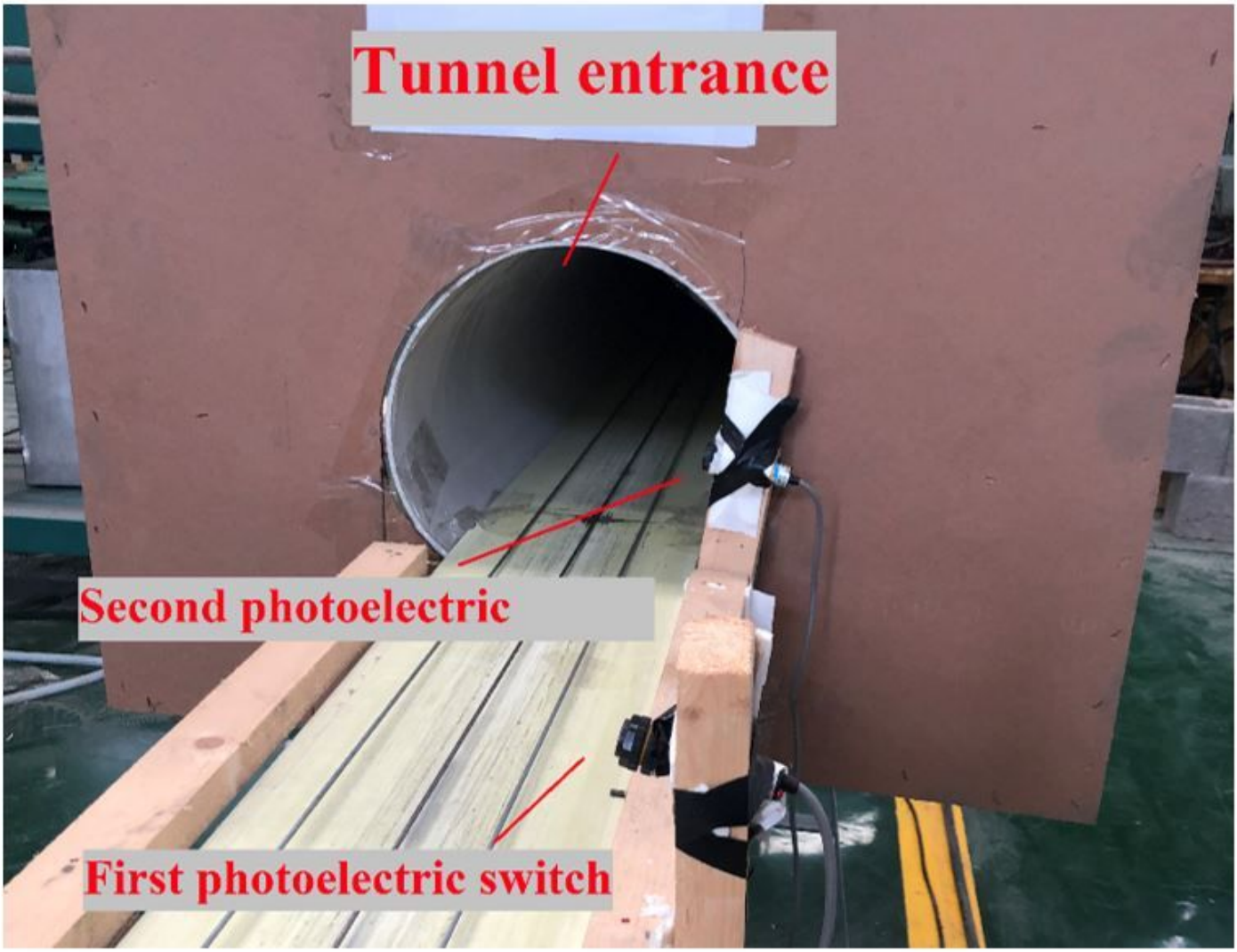

Figure 5

Sensors at tunnel entrance

(a) Sensor at tunnel exit (b) The buffer structure of tunnel exit

Figure 6

Damping system of the model test bench

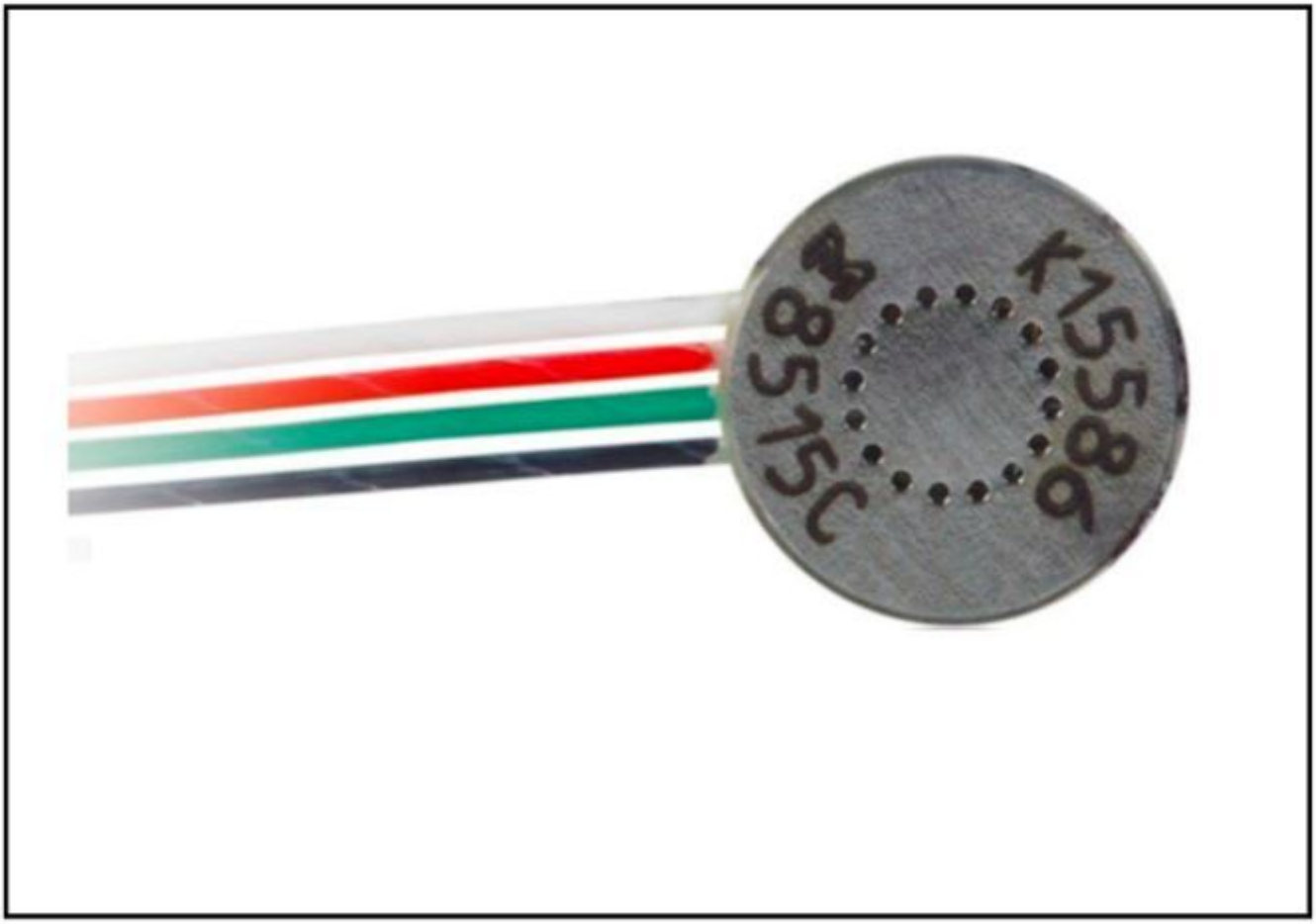

Figure 7

Pressure sensor Endevco 8515C-15

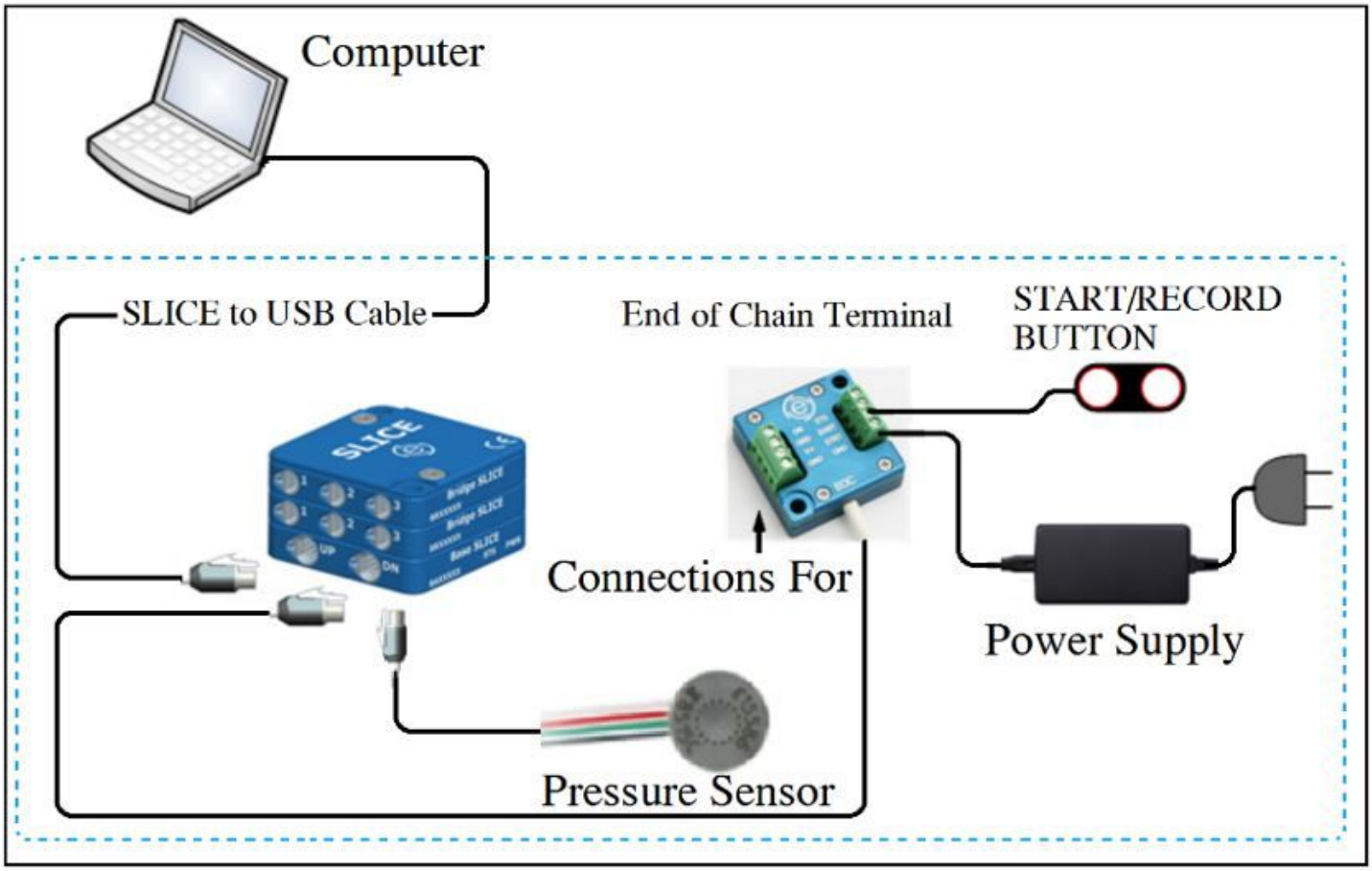

Figure 8

Data acquisition system SLICE

Figure 9

Photoelectric switch

Figure 10

The interface of PLC control system

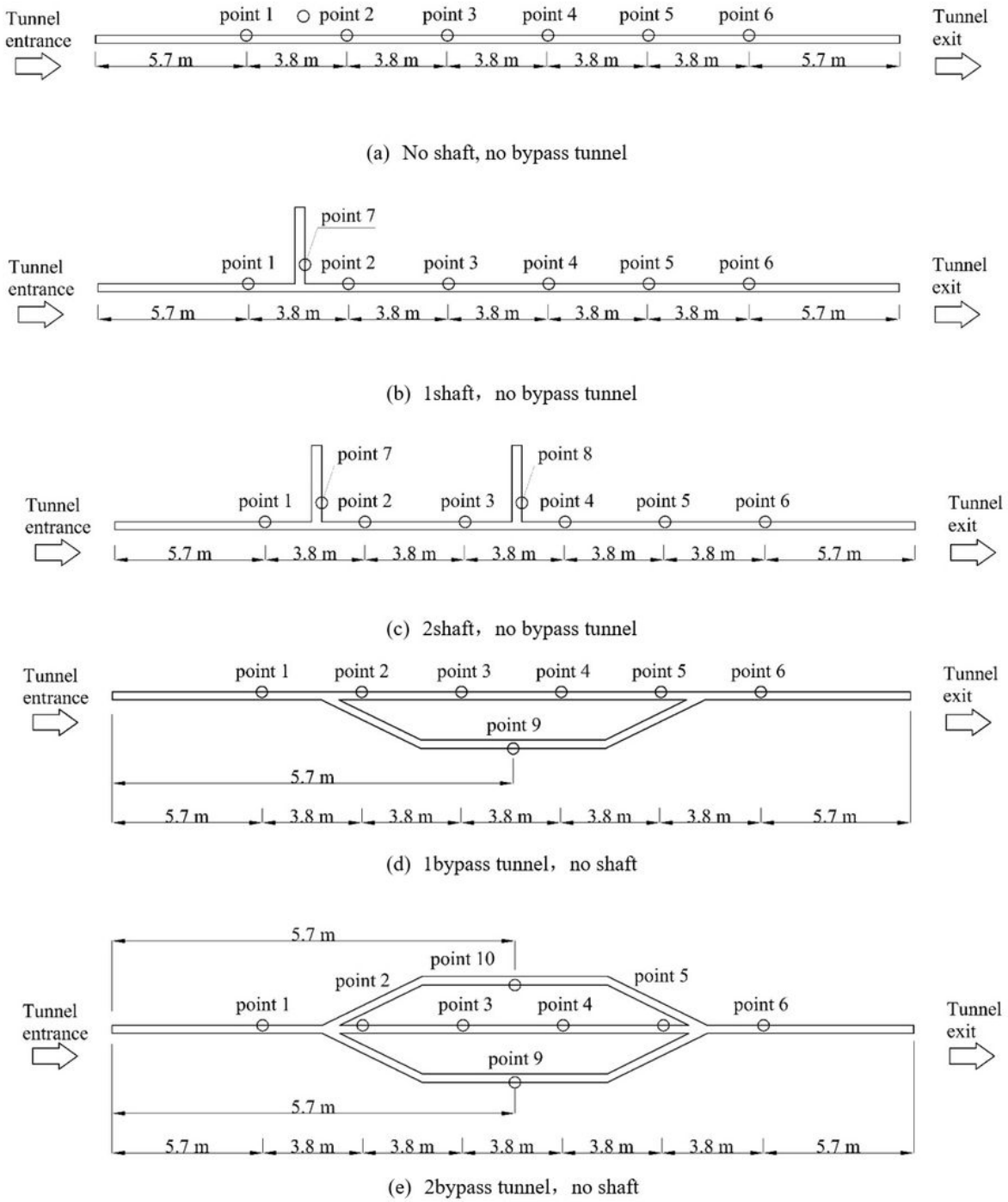

Figure 11

Layout of measuring points in tunnels (the circles in the figure are the measuring points arranged)

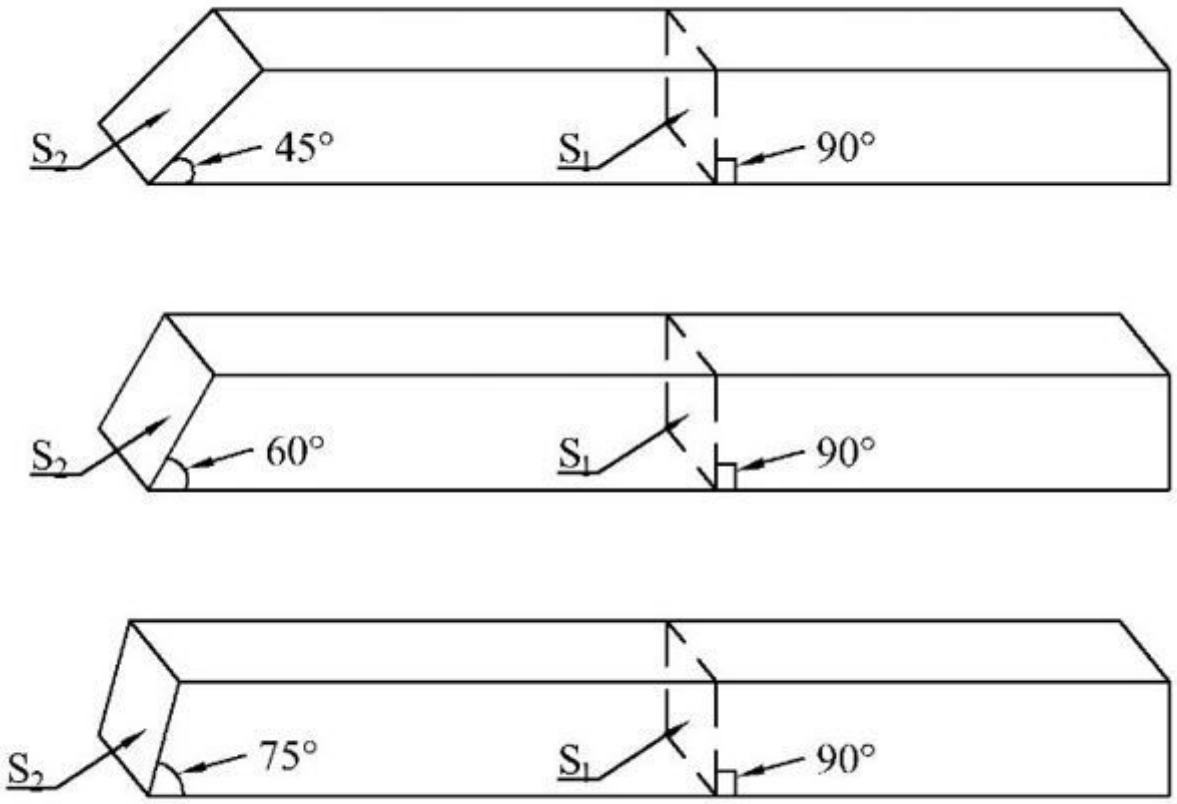

Figure 12

Comparison of locomotive of different shapes

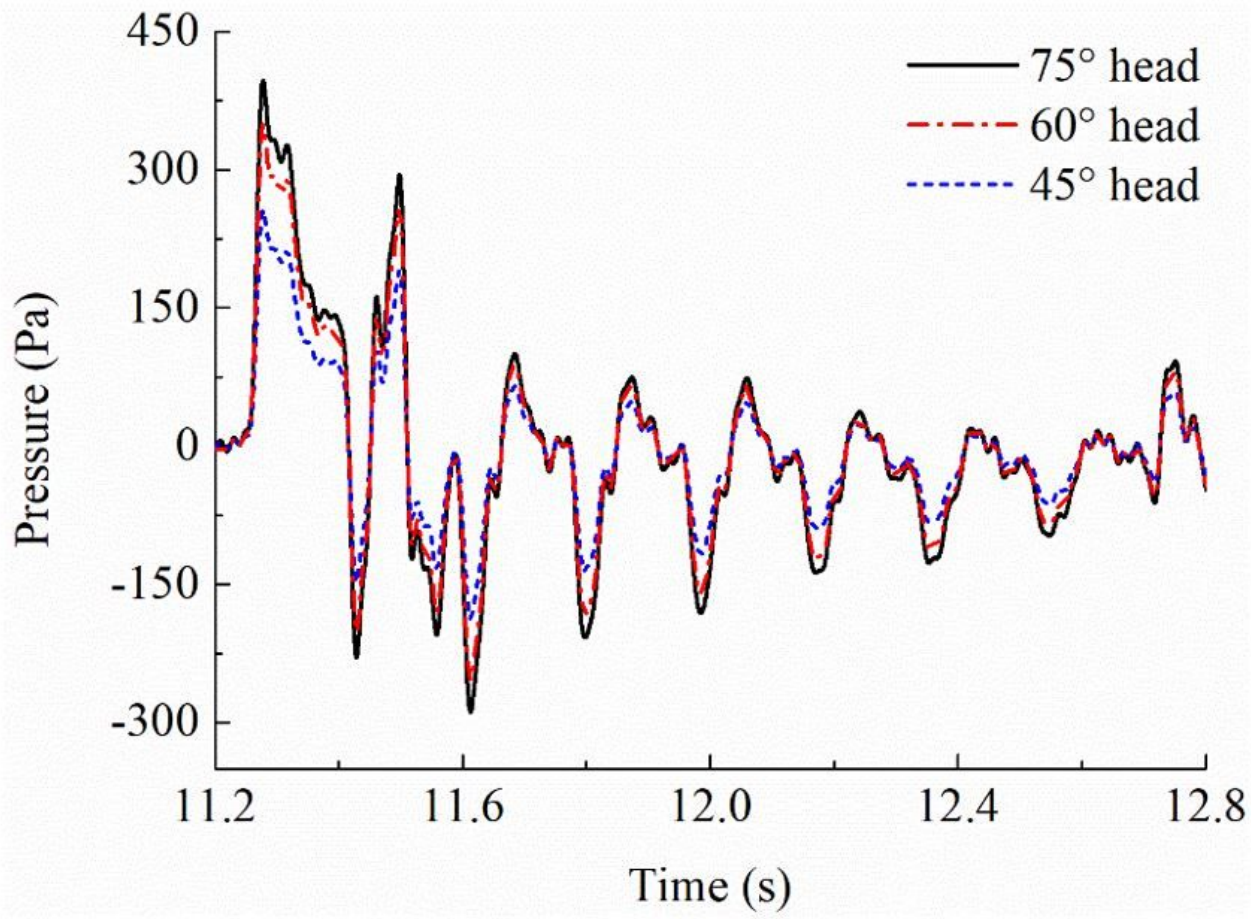

Figure 13

Comparison of dynamic pressure changes at measuring point 1

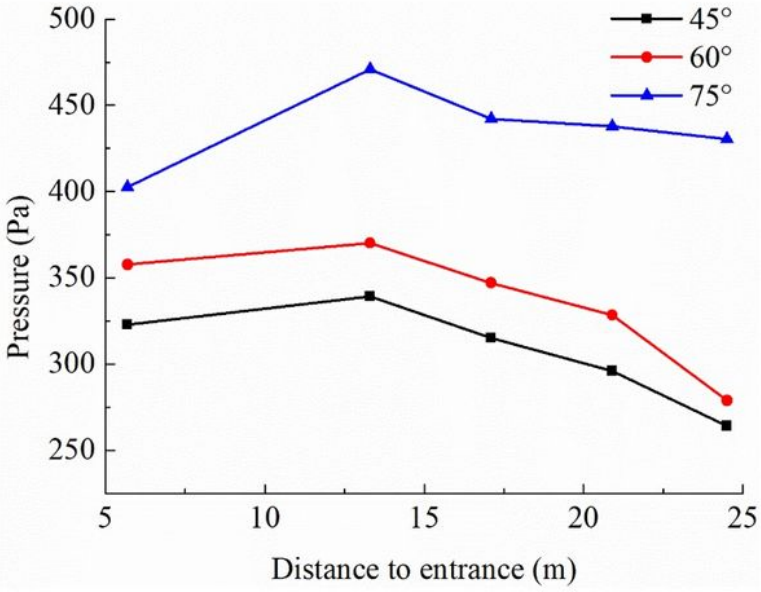

(a) Positive pressure

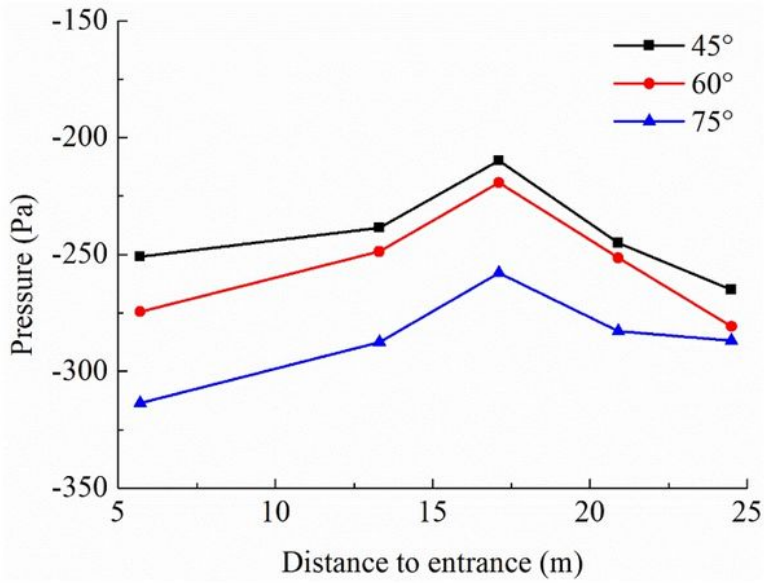

(b) Negative pressure

Figure 14

Peak pressure generated by train models with different head shapes

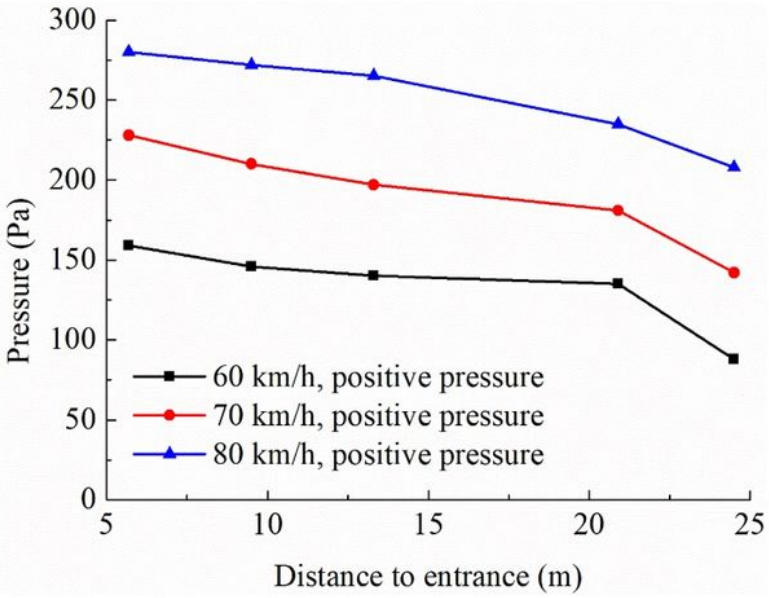

(a) Positive pressure value

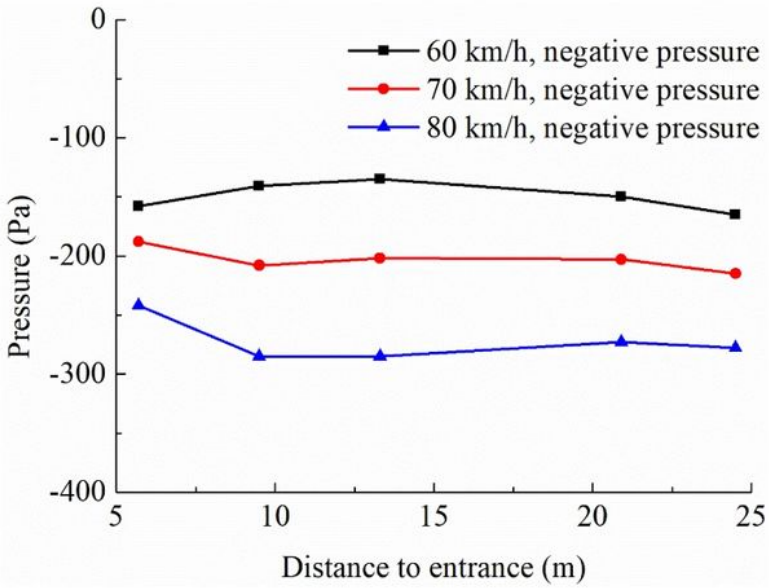

(b) Negative pressure value

Figure 15

Pressure peaks generated by the model car under different speed cases

Figure 16

Pressure fluctuation analysis diagram

Figure 17

Pressure peak fitting diagram

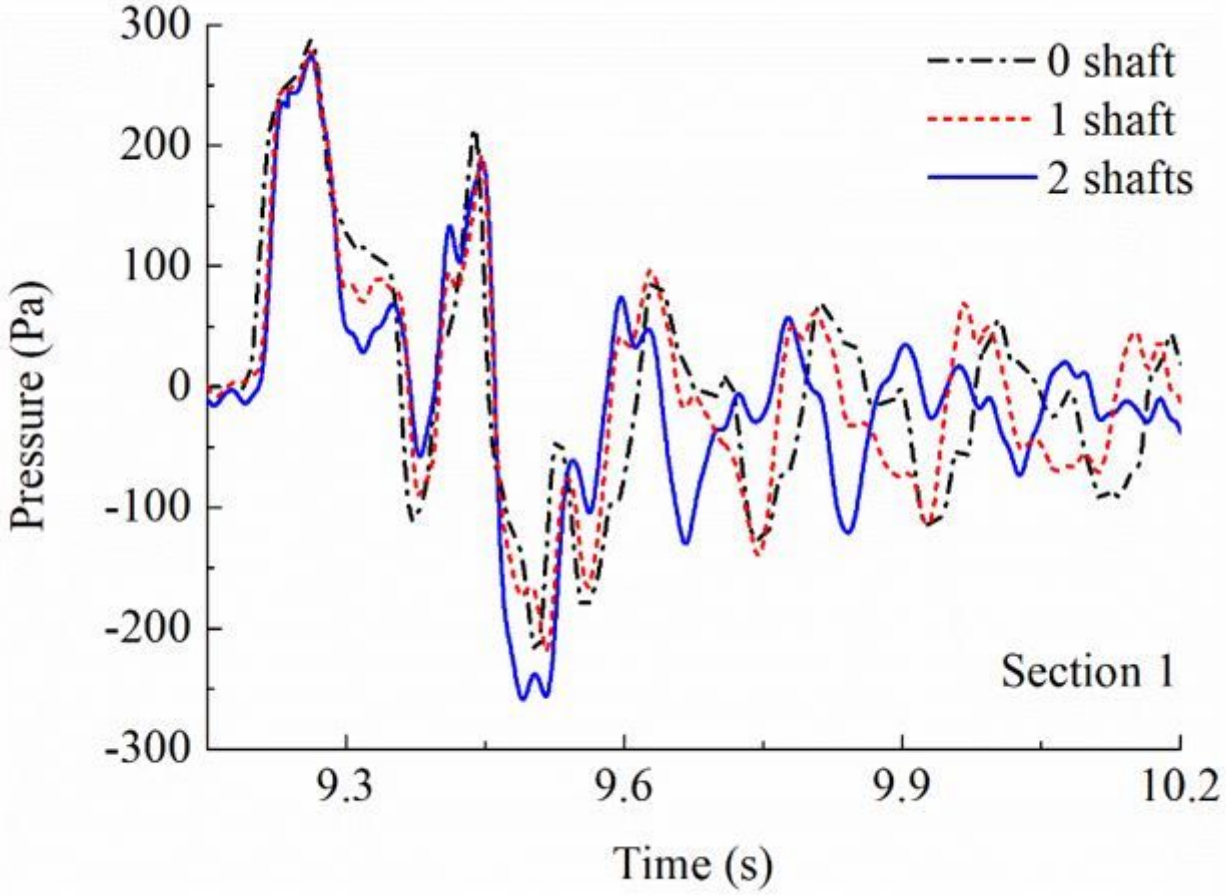

Figure 18

Comparison of dynamic pressure changes at measuring point 1

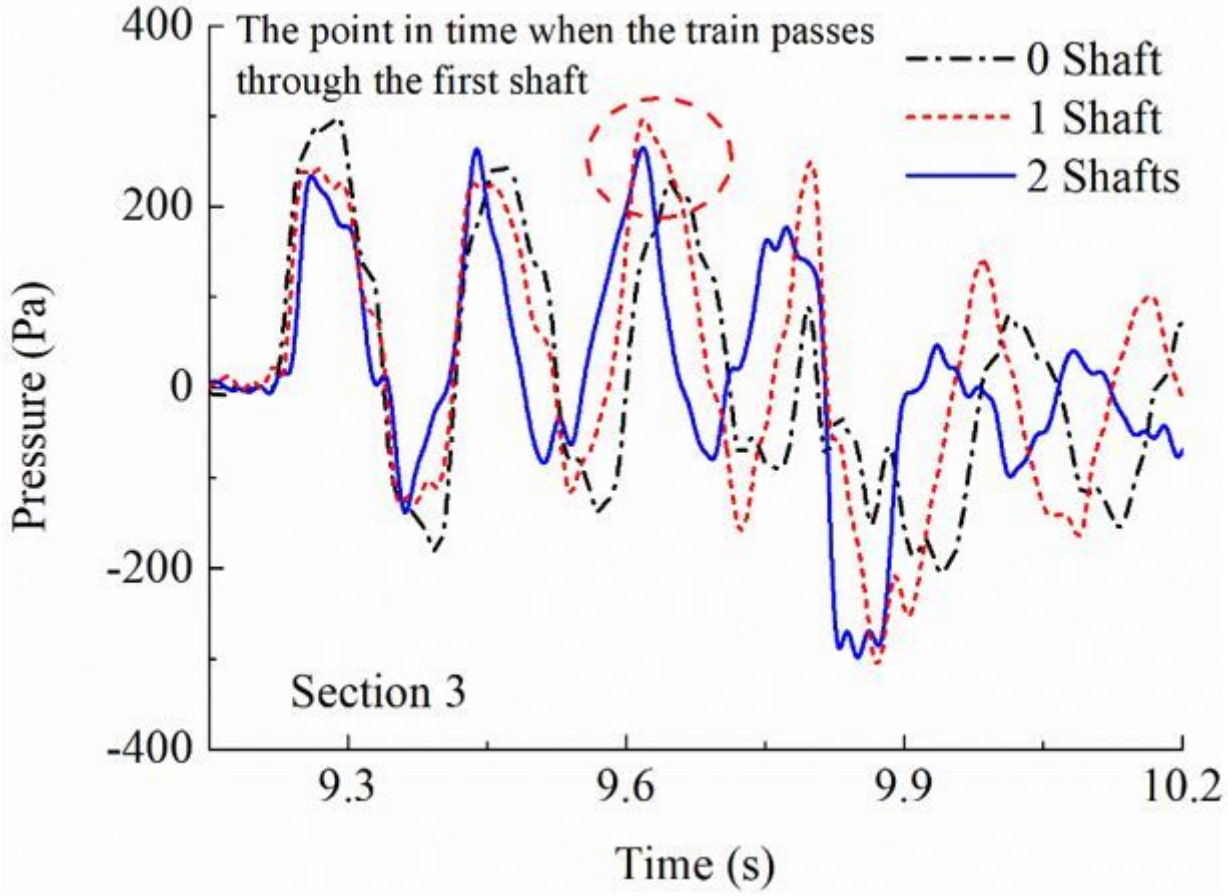

Figure 19

Comparison of dynamic pressure changes at measuring point 3

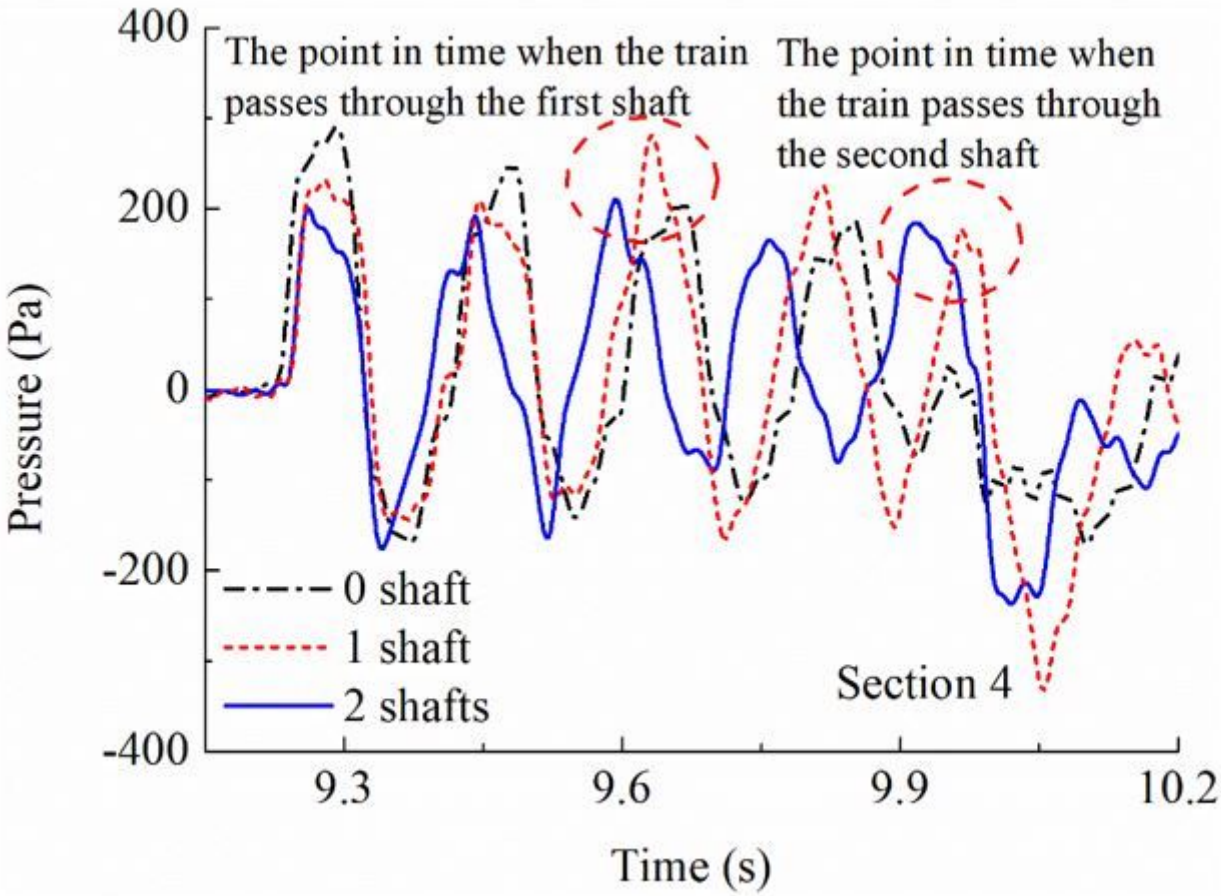

Figure 20

Comparison of dynamic pressure changes at measuring point 4

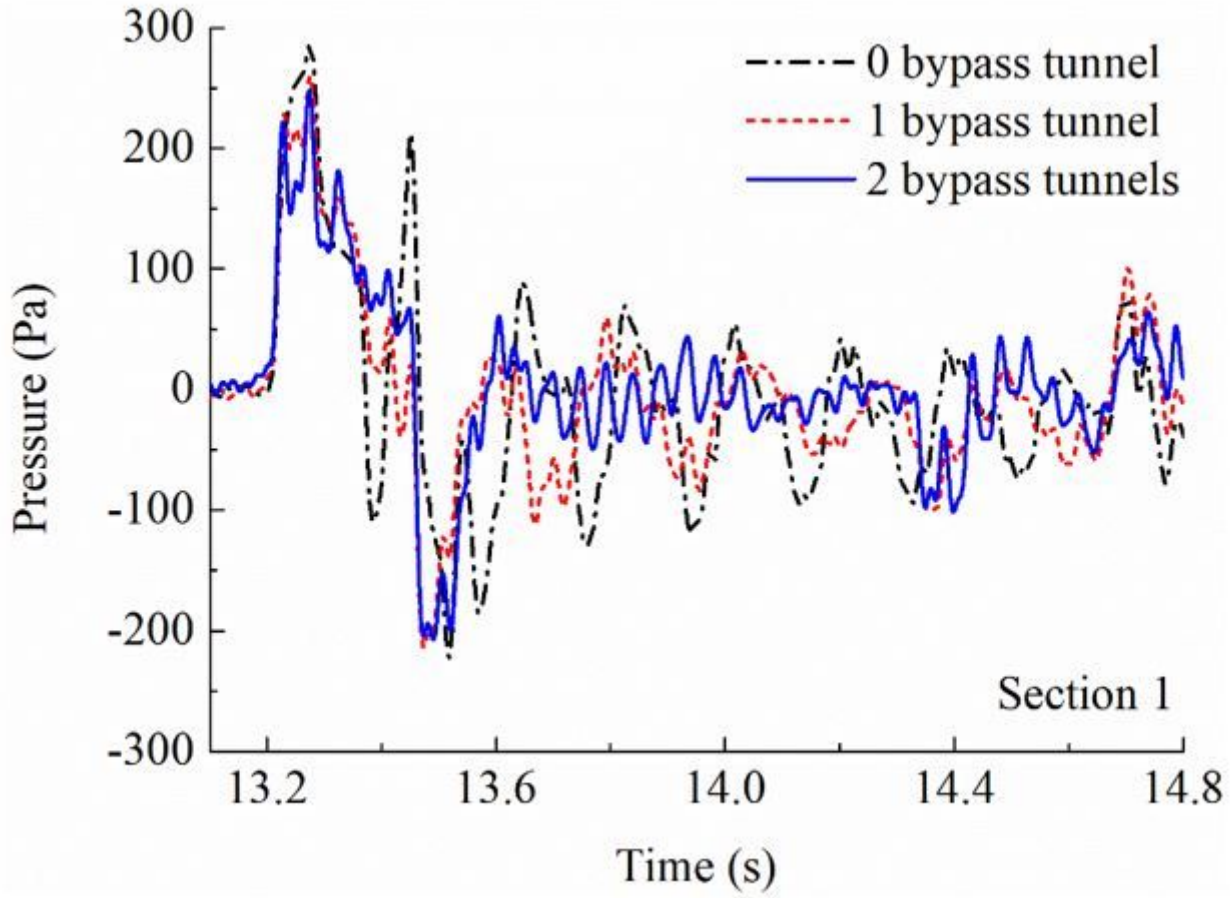

Figure 21

Comparison of dynamic pressure changes at measuring point 1

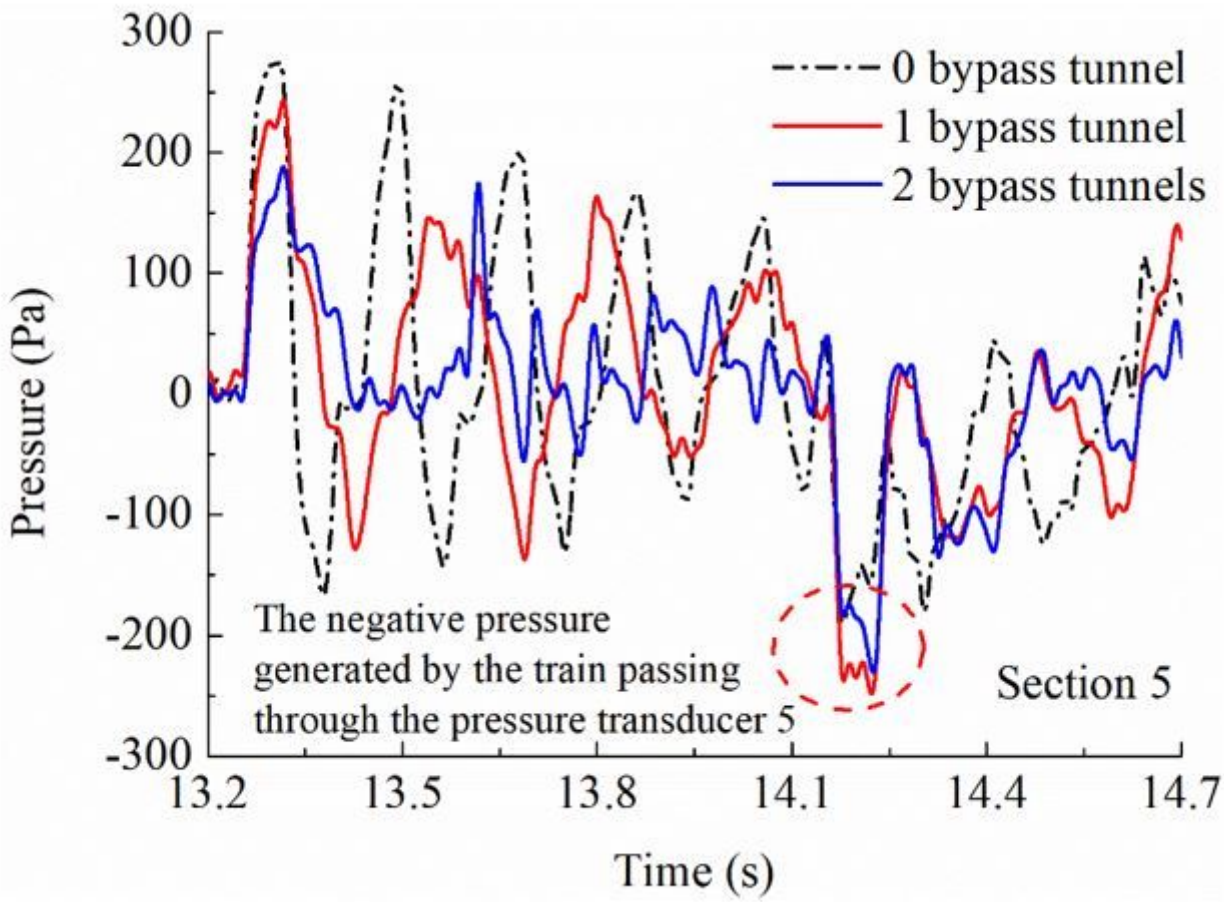

Figure 22

Comparison of dynamic pressure changes at measuring point 5

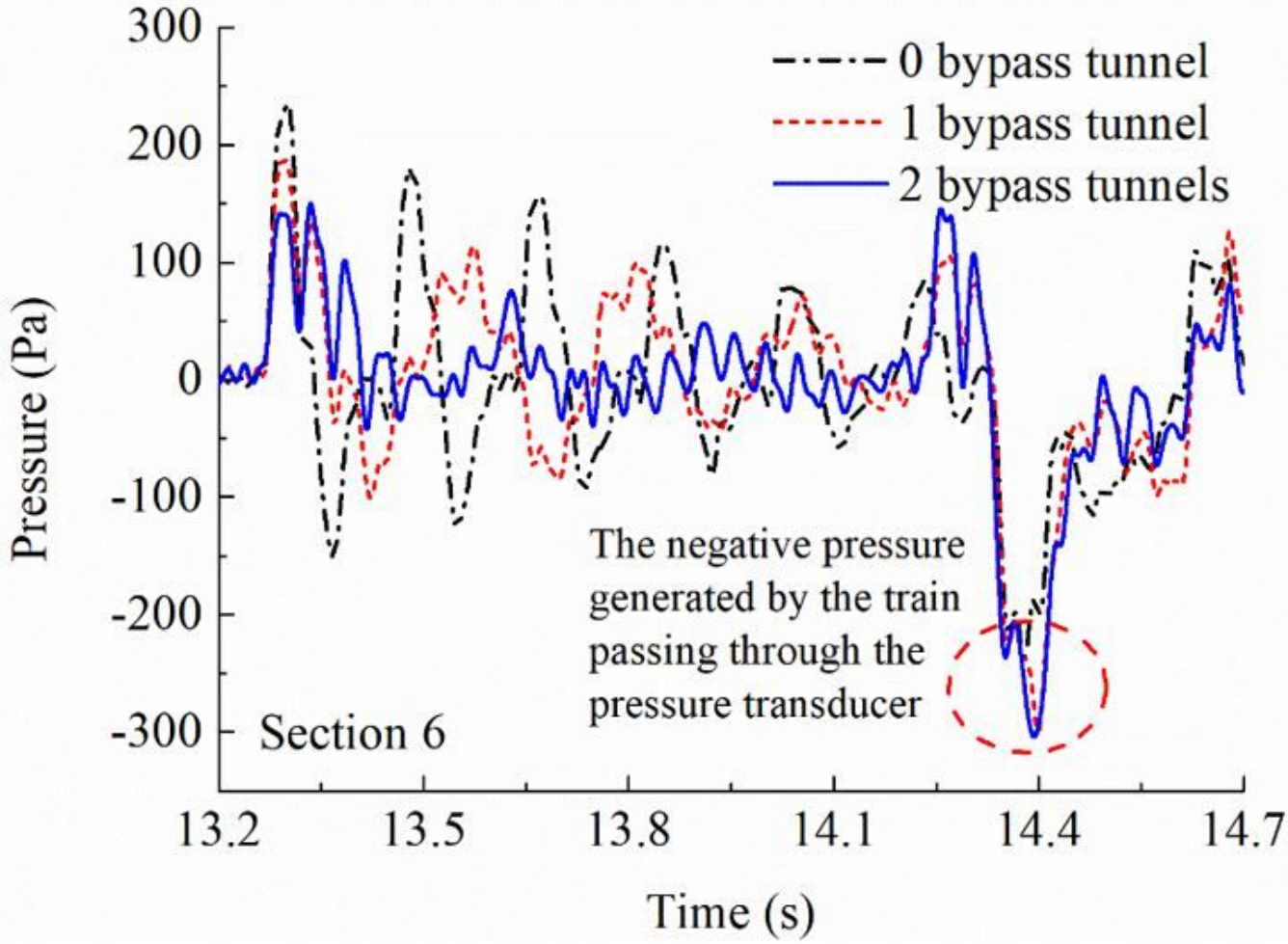

Figure 23

Comparison of dynamic pressure changes at measuring point 6

Supplementary Files

This is a list of supplementary files associated with this preprint. Click to download.

- Tables.docx